Nanoscale carbon blacks produced by CO_2 laser pyrolysis

Xiang-Xin Bi[a)]
Center for Applied Energy Research, University of Kentucky, Lexington, Kentucky 40511–8433 and Department of Electrical Engineering and Computer Science, Massachusetts Institute of Technology, Cambridge, Massachusetts 02139

M. Jagtoyen
Center for Applied Energy Research, University of Kentucky, Lexington, Kentucky 40511–8433

M. Endo
Faculty of Engineering, Shinshu University, Nagano-city 380, Japan

K. Das Chowdhury[b)]
Department of Materials Science and Engineering, Massachusetts Institute of Technology, Cambridge, Massachusetts 02139

R. Ochoa and F. J. Derbyshire
Center for Applied Energy Research, University of Kentucky, Lexington, Kentucky 40511–8433

M. S. Dresselhaus
Department of Electrical Engineering and Computer Science and Department of Physics, Massachusetts Institute of Technology, Cambridge, Massachusetts 02139

P. C. Eklund
Center for Applied Energy Research, University of Kentucky, Lexington, Kentucky 40511–8433 and Department of Physics and Astronomy, University of Kentucky, Lexington, Kentucky 40506

(Received 16 February 1995; accepted 30 June 1995)

CO_2 laser pyrolysis has been used to synthesize carbon black (particle diameter ~30 nm) via a catalytically driven pyrolysis of benzene vapor. The H : C ratio is found to be ~1 : 10, which is unusually high for carbon blacks. Subsequent heat treatment of the "laser black" to temperatures up to ~2800 °C produces well-graphitized faceted particles with central polygonal cavities. High resolution TEM lattice imaging, Raman scattering, and x-ray diffraction have been used to characterize the morphological structure of these carbon particles in their as-synthesized and heat-treated forms. Furthermore, KOH treatment at ~800 °C has been employed to activate the as-synthesized particles, producing a tenfold increase in the surface area from 50 to 700 m^2/g. Possible pore structures generated during this activation process have been identified by high resolution TEM imaging.

I. INTRODUCTION

Classical carbon blacks represent many morphological forms of finely divided carbon-based particles with diameters in a typical range of 10–100 nm. They are often produced by hydrocarbon dehydrogenation with, or without, the assistance of a catalyst.[1] They have been studied, and widely used as a filler to modify the mechanical, electrical, and optical properties of the host material (e.g., rubber tire).[2] Different types of industrial carbon blacks have been given names that in many cases are derived from the processes by which they are prepared. For example, "thermal blacks" were produced by thermal decomposition of natural gas, "channel blacks" by partial combustion of natural gas, "acetylene blacks" by exothermic decomposition of acetylene, "furnace blacks" by partial combustion of oil droplets, and "plasma blacks" by decomposition of ethylene in a plasma arc.[1] On a laboratory bench scale, carbon blacks have also been prepared by special processes such as laser ablation of graphite,[3] CO_2 laser pyrolysis of acetylene,[4,5] and heat treatment of coal in air.[1] Most recently, carbon arc discharges[6] used to produce fullerenes have also been shown to produce nanoscale carbon blacks, yet with a rather large particle size distribution. The above-mentioned variety of synthesis routes have produced carbon blacks with notably different physical (e.g., surface area, morphology) and chemical (surface functional groups, incorporated metals) properties, which have been tailored for different applications in industry.

[a)]Present address: International Center for Materials Research, 750 Enterprise Dr., Lexington, Kentucky 40511.
[b)]Present address: Intel Corp., 4100 Sara Rd., Rio Rancho, New Mexico 87124.

The synthesis of carbon blacks involving a CO_2 laser was first carried out by Yampolskii *et al.*,[4] and later by Maleissye *et al.*[5] In their studies, carbon blacks were obtained by decomposing acetylene (C_2H_2) gas using a CO_2 laser as a heating source. No detailed studies were performed to characterize the physical properties of these carbon blacks in either the as-synthesized or heat-treated forms. In this study, we have produced carbon black particles from an ethylene/benzene mixture using a CO_2 laser pyrolysis technique.[7] Recently, we have also used this technique to produce a wide range of metal carbide, nitride, sulfide, and oxide nanocrystalline particles of 5–20 nm in diameters.[8–12] As we discuss in more detail below, a CO_2 laser beam was used to pyrolyze benzene (C_6H_6) in the presence of a small amount of iron carbonyl $Fe(CO)_5$ which serves as a catalyst. Ethylene (C_2H_4), which has molecular vibrational/rotational bands that match the CO_2 laser energy, was also present to absorb CO_2 laser radiation and thereby to sustain the reaction. Using high resolution transmission electron microscopy (TEM) imaging, we found the as-synthesized particles to be nearly spherical (average diameter ~30 nm) and nearly amorphous. Upon heat-treating these particles up to 2800 °C, we obtained well-graphitized, hollow particles with a polyhedral shape. Furthermore, using a KOH activation process, we achieved a 10-fold increase in the specific surface area for these particles, from ~50 m^2/g to ~700 m^2/g.

The CO_2 laser pyrolysis (LP) technique,[7] as shown in Fig. 1, has a small reaction zone defined by the overlap between the vertical reactant gas stream and the horizontal laser beam. The reaction zone is safely away from the chamber walls. This unique design provides an ideal environment to grow small particles in the nanometer range, with less contamination and a narrower size distribution than those prepared by conventional thermal methods which involve hot furnace walls in contact with the reactant gases. In the case of carbon black synthesis, this technique offers another benefit; that is, LP generates only carbon black particles from the nuclei formed *directly* in the reaction zone. This is because the reaction chamber remains at room-temperature during the synthesis, and the possible generation of pyrolytic carbons from hot chamber walls is eliminated. Particle generation on hot furnace walls is well known to be an important process which competes with particle nucleation and growth from the gas phase.[1] The unavoidable mixing of these two very different particles has hindered the development of models for the formation of carbon black. Many studies by Tesner *et al.*[13–15] and Fedoseev and Vnukov[16] were devoted to this issue. Finally, it should be mentioned that the CO_2 laser pyrolysis production of carbon black (or laser black) closely resembles the flame synthesis process, but does not require the presence of oxygen to initiate or sustain the reaction.

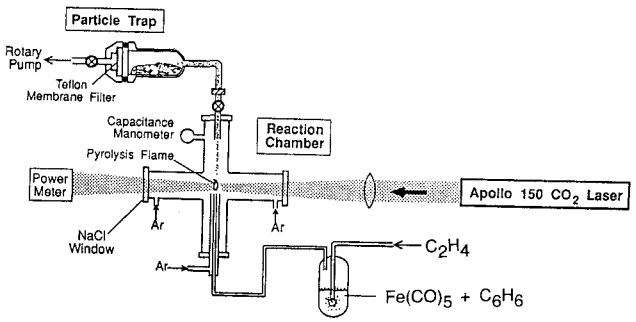

FIG. 1. CO_2 laser pyrolysis system for the synthesis of metal oxide, nitride, sulfide, or carbide nanoscale particles. The specific reagents shown are for the production of carbon blacks.

The morphological nature of several types of carbon blacks in their as-synthesized and heat-treated (up to 3000 °C) forms has been established mainly by x-ray diffraction (XRD) and high resolution TEM lattice imaging.[1,17,29] The earliest XRD studies on carbon blacks by Warren[17,18] indicated that most as-synthesized carbon blacks were amorphous, except for some small inclusions of graphitic regions. They proposed a means of characterizing the degree of graphitization in carbon blacks by determining the dimensions of these graphitic regions, measured by L_a and L_c, where L_a is the crystalline length in the basal plane, and L_c is the thickness of the graphitic region over which the ABAB...stacking of the carbon layers remains intact. These two characteristic lengths were determined by Warren using the Debye–Scherrer formula relating crystallite size to the XRD linewidth. This simple scheme for describing the degree of graphitization in carbon blacks was confirmed by Hall[27] using direct high resolution TEM lattice imaging. The parameters L_a and L_c provided a simple and useful base and have been used frequently in later studies on industrial carbon blacks, including thermal blacks, channel blacks, acetylene blacks, plasma blacks, and furnace blacks.[23] The correlation between structural disorder and lattice spacing d_{002} in carbon blacks was also established by Franklin[19,20] in the early 1950s.

Another characteristic signature of carbon blacks is the quasi-concentric organization of curved carbon layers within a particle, as identified in high resolution TEM imaging.[2,27–30] These concentric graphene layers were found to be more evident near the particle surface than near the particle center. Their appearance was also found to correlate with particle size, synthesis time, and temperature. Similar to our results, studies on morphological changes induced in the as-synthesized carbon blacks by heat treatment in Ar up to 3000 °C found the tendency to form polyhedral-shaped particles with an empty central core and a well-graphitized carbon shell.[2,25,26,31,32]

Raman scattering was first used systematically by Tuinstra and Koenig[33] to characterize several related forms of carbons with sp^2 bonding, including single-crystal graphite, pyrolytic graphite, activated charcoal, and carbon blacks. In their studies all the carbon samples were found to exhibit two prominent Raman bands, one at ~1575 cm^{-1} and the other at ~1355 cm^{-1}. The first one (1575 cm^{-1}) is assigned to an in-plane graphitic E_{2g} symmetry mode vibration, which is observed at 1582 cm^{-1} in single-crystal graphite.[34] The second broader band (1355 cm^{-1}) is identified with an *in-plane,* disorder-induced isotopic feature. It is interesting that the authors observed a close correlation between the in-plane crystalline size L_a and the ratio of the integrated intensity of these lines. The correlation, $L_a \sim 44(I_{1575}/I_{1355})$ Å for 4880 Å laser excitation, was later found to apply in other carbon materials, including carbon fibers.[35,36] Recent studies have shown that diamond-like carbons also exhibit a broad peak at ~1332 cm^{-1}, but in this case, the band is identified with sp^3 bonded carbons and is associated with disorder-induced broadening of the narrow, first-order Raman-allowed line at 1335 cm^{-1} of crystalline diamond. Diamond-like carbons also often exhibit a broadband near 1580 cm^{-1}, which is interpreted as evidence for sp^2 bonded graphitic inclusions in the diamond-like structures. Furthermore, since the cross section σ for Raman scattering for sp^2 and sp^3 bonded carbons is rather different ($\sigma_{sp^2} \gg \sigma_{sp^3}$),[34] it becomes difficult to determine each individual contribution to the two composite Raman peaks. Therefore, if the carbon black samples contain a significant amount of sp^3 bonded carbon species, or if the laser excitation wavelength differs from 4880 Å, the correlation between the crystalline size L_a and I_{1575}/I_{1355} may become invalid. Nevertheless, measurement of these two Raman lines is useful to monitor the graphitization process of mostly sp^2 bonded carbons upon heat treatment at elevated temperatures.

II. SYNTHESIS

Carbon black samples were produced in gram quantities using the CO_2 laser pyrolysis system shown schematically in Fig. 1, which is similar to that described previously by Haggerty.[7] The reactant species, including $Fe(CO)_5$ (99.9%) and C_6H_6 (HPLC grade), were introduced into the reactant gas stream by bubbling C_2H_4 (99.99%) gas through a diffuser into a solution of benzene mixed with the iron carbonyl mixture [$C_6H_6 : Fe(CO)_5 = 50:1$, by volume] contained in a glass container (Fig. 1). The reactant gases then passed vertically out of a stainless steel nozzle (diameter = 6 or 9 mm) inside the 6-way stainless steel cross (chamber) and intersected a horizontal CO_2 laser beam (Laser Photonics Model 150). The overlap between the laser beam and the reactant gas stream defines a small reaction zone, protected by a coaxial flow of high purity Ar gas (99.999%). The energy coupling of the laser to the reactant gases is realized by tuning the laser frequency to the ethylene P20 line (945 cm^{-1}), which is shifted by 5 cm^{-1} relative to the strongest nearby rotational-vibrational absorption line of ethylene at 950 cm^{-1}. A ZnSe lens was used to adjust the position of the CO_2 laser beam waist relative to the nozzle tip. The ethylene flow rate was regulated by a mass flow controller, and the chamber pressure was controlled by adjusting a needle valve located between the reaction chamber and a mechanical vacuum pump.

During the steady-state production of laser black, a stable, bright white reaction flame could be observed in the reaction zone just above the nozzle. After leaving the pyrolysis zone, these particles could be seen to drift upward in a well-collimated ~3 mm diameter stream in the center of the 1 cm (i.d.) glass tube connecting the 6-way stainless steel cross and the Pyrex particle trap. This confinement of the particle stream was realized by the coaxial Ar flow introduced in a tube surrounding the reactant gas nozzle, and by the symmetrical design of our system (Fig. 1). Importantly, Ar gas is also delivered to the laser entrance and exit windows to sweep away any stray particles that might find their way onto the windows. These particles can cause permanent damage to the NaCl salt windows when illuminated with an intense infrared laser beam. Typical values of reaction parameters used in the synthesis of our laser black particles were as follows: laser intensity ~110 W, chamber pressure ~300 Torr, C_2H_4 flow rate ~300 sccm, and reactant gas nozzle diameter N_D ~6 mm. A 9 mm nozzle is also used to produce laser black particles for study of the KOH activation process.

The elucidation of the gas phase chemistry leading to the nucleation and growth of the laser black particles is complicated by the presence of several carbon-containing species in the reaction zone, including ethylene, benzene, and the carbon monoxide liberated from the iron pentacarbonyl. To elucidate the carbon chemistry, we have carried out several LP reactions using different mixtures of reactant gases, while keeping other reaction parameters the same. First, if only ethylene (no benzene and iron carbonyl) was introduced into the reaction zone, we observed neither carbon black formation nor a clear reaction flame in the reaction zone. Second, if only benzene and ethylene (no iron carbonyl) were introduced into the reaction zone, we again did not see any formation of carbon blacks. Third, as reported in our previous work,[9] if only ethylene and iron carbonyl (no benzene) were pyrolyzed, the reaction products were found to be single-crystal iron carbide particles (Fe_3C or

Fe_7C_3). These particles exhibit a coating of a few monolayers of pyrolytic carbon. In contrast to the bright white flames we observed in the production of laser black, we could observe only a very dim reaction flame while producing Fe carbides. Only with the presence of all three components (i.e., C_2H_4, C_6H_4, C_6H_6, and $Fe(CO)_5$) could we see significant laser black production. Typical laser black production rates observed in our current system were ~1 g/h. Since the laser black was produced even if very small amounts of $Fe(CO)_5$ were present in the reactant gas stream, we conclude that very small Fe particles were formed from dissociated $Fe(CO)_5$, and these particles serve as a catalyst in the synthesis process.

Other evidence of the catalytic effect of Fe particles in the production of carbons is extensively documented in the literature.[37,38] In fact, it has been reported that iron catalysts (e.g., α-Fe particles) exhibit higher catalytic activity for soot formation than do other transition metal catalysts, such as Co or Ni. The activity has been associated with the formation of highly dispersed iron crystallites embedded in the carbon particle or product. No general agreement regarding the mechanism for the formation of carbon black particles has been reached. One popular view, consistent with the available experimental evidence, involves condensation reactions of aromatic rings through radical or ion intermediates.[39,40] These reactions produce carbons from polyaromatic hydrocarbon molecules, accompanied by simultaneous loss of hydrogen.

The structural form of the carbon produced by the catalytic decomposition of linear chain and aromatic hydrocarbons over metal catalysts has been found to be dependent on synthesis conditions.[39] For example, the production of amorphous, filamentous, and graphitic carbons from the decomposition of acetylene on small iron, cobalt, and nickel particles (~10 nm) has been reported by Baker *et al.*,[38] who found that the form of the carbon produced depended essentially on the temperature (500–1000 °C) at which the acetylene decomposed. They suggested that in the production of amorphous carbon, which proceeded at about 500 °C, the reaction occurs essentially in the gas phase and the iron catalyst acted as a nucleating agent for carbon particle formation. Higher temperature reactions resulted in the production of filamentous and graphitic carbon. It should be noted that the estimated temperature in laser pyrolysis is usually of the order ~800–1000 °C.[7] As discussed below, the carbon particles produced by LP are decidedly amorphous, as determined by TEM studies. The amorphous character of the laser black particles may be due to the high heating and cooling rates involved in the LP synthesis.

III. LASER BLACK PROPERTIES

A. High resolution TEM lattice imaging

Shown in Figs. 2(a) and 2(b) are, respectively, overview (200,000×) and close-up (1,000,000×) images of the as-synthesized particles taken by high resolution, phase contrast imaging, using a JEOL 4000 electron microscope (200 kV). High resolution images were taken using a standard phase contrast technique.[27]

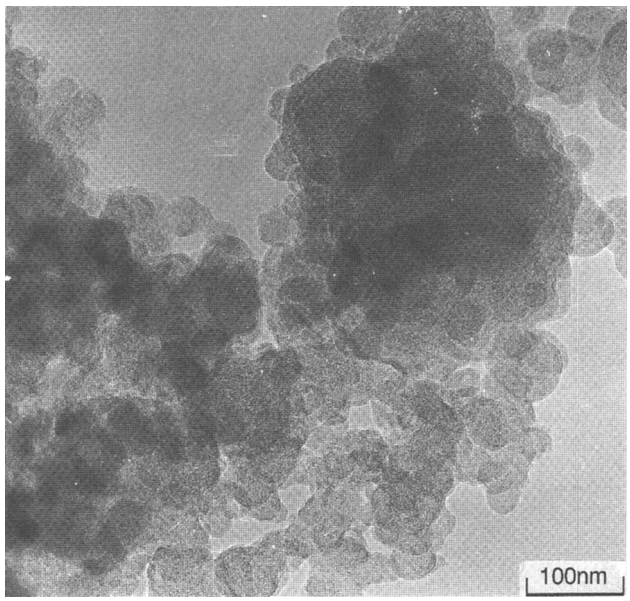

(a)

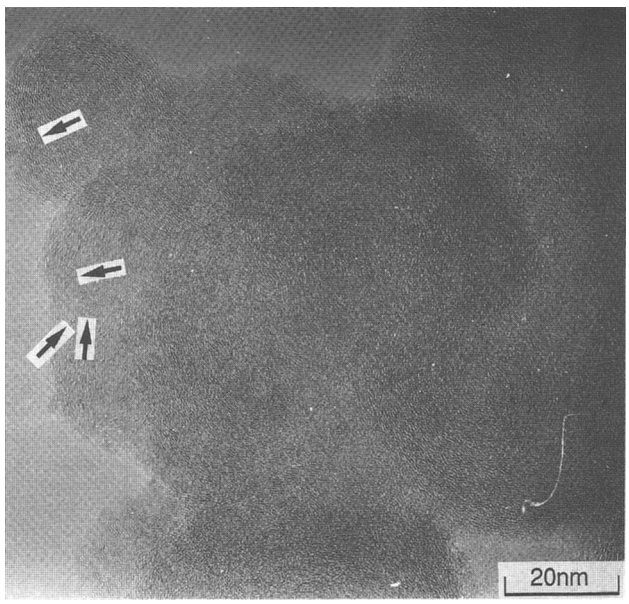

(b)

FIG. 2. High resolution TEM overview (a) and close-up (b) images of as-synthesized laser black particles. Graphitic regions are indicated by arrows.

The overview picture was taken to reveal the average surface morphology, particle sizes, distribution, and particle agglomeration. The higher resolution image [Fig., 2(b)] reveals details concerning the carbon atom organization within the particle and near the surface. As shown in Fig. 2(a), the carbon black particles present, on average, a spherical shape, with an average particle diameter on the order of ~30 nm. Accurate determination of the particle size and size distribution was difficult due to particle agglomeration on the TEM grid and possible interparticle fusion occurring during the LP process. The high resolution image [Fig. 2(b)] indicates that the laser black particles are a highly disordered graphitic carbon. The formation of parallel, yet curved, graphene layer segments is observable near the surface of a few particles The overall atomic disorder within the particles observed for our laser black appears to be more significant than observed in common thermal black.[1,2,21] From Fig. 2(b), we have measured the spacing between graphene layers in several regions, and obtained values in the range of 0.38–0.42 nm. It should be noticed that these values of d_{002} are large relative to those obtained for many industrial carbon blacks,[2] consistent with a higher degree of disorder in our as-synthesized particles. This may stem from either the low flame temperature or the rapid heating and cooling of the particles in the laser beam. Although we have not measured the temperature of this specific LP reaction, previous T-measurements by Haggerty[7] arrive at estimates of ~1000–1200 K as typical values.

In Figs. 3(a) and 3(b), we display the TEM images of the laser black particles heat-treated at a heat-treatment temperature (HTT) = 2000 °C in flowing Ar gas. It is clear from the overview picture [200,000×, Fig. 3(a)] that the particles have maintained their individual identity, and no evidence is seen for significant sintering. The close-up view [1,000,000×, Fig. 3(b)] of the HTT = 2000 °C particles does show the development of a more ordered graphitic carbon layer structure in the region near the particle surface. As found in the as-synthesized particles, the curved carbon layers align with the particle surface. The average lattice spacing d_{002} for the HTT = 2000 °C laser black particles is 0.39 ± 0.02 nm.

We next show the overview (200,000×) [Fig. 4(a)] and close-up (1,000,000×) [Fig. 4(b)] images taken on the laser black exposed to a HTT = 2850 °C. For HTT = 2850 °C, the particles have lost the approximate spherical shape observed in their as-synthesized form, and the particles now exhibit a new morphology comprised of a polyhedral outer shell with a faceted surface and an empty hollow polyhedral center. It appears that the shell is well graphitized, with an average shell thickness of ~7 nm. The interplanar spacing d_{002} between those graphitic planes is now ~0.37 ± 0.02 nm, reduced from the value (0.39 nm) observed in the 2000 °C treated particles. As indicated in Fig. 4(b), it is interesting to see that inside the graphitized carbon particles, there exist a second shell consisting of 2–5 monolayers. Furthermore, from these three sets of images, Figs. 2, 3, and 4, it appears that with increasing HTT, the regions near the particle surface graphitize initially. This is attributed to the formation of lower energy, flat graphitic facets which necessarily produce a void in the center of the polyhedron.

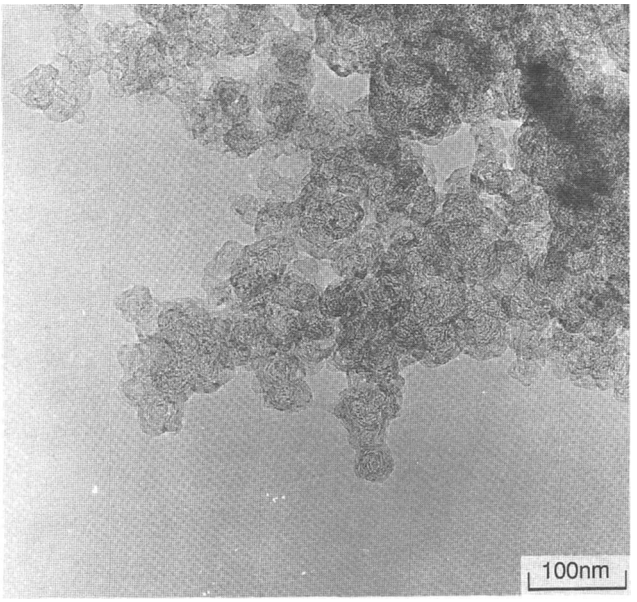

(a)

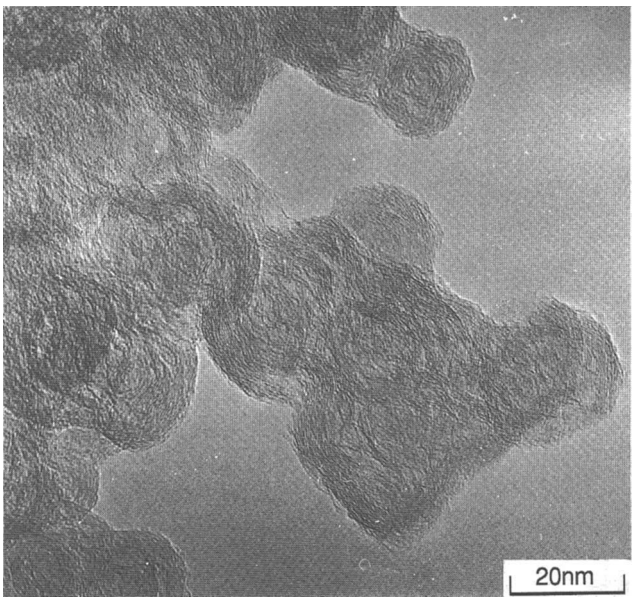

(b)

FIG. 3. High resolution TEM overview (a) and close-up (b) images of laser black particles heated to a HTT = 2000 °C in Ar.

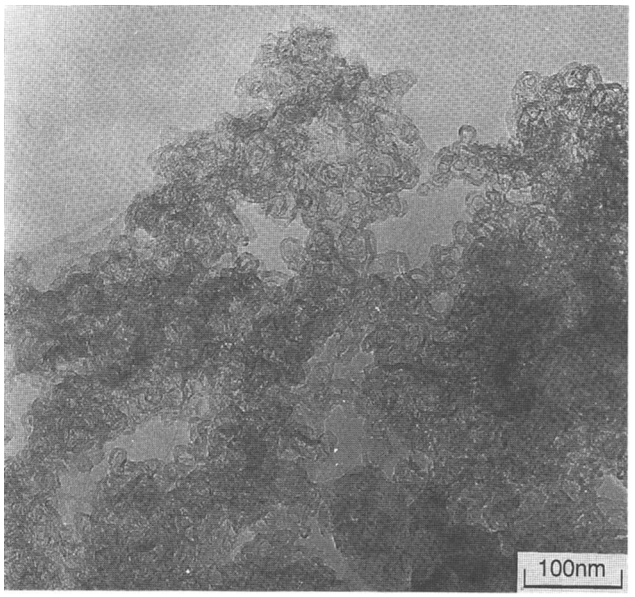

(a)

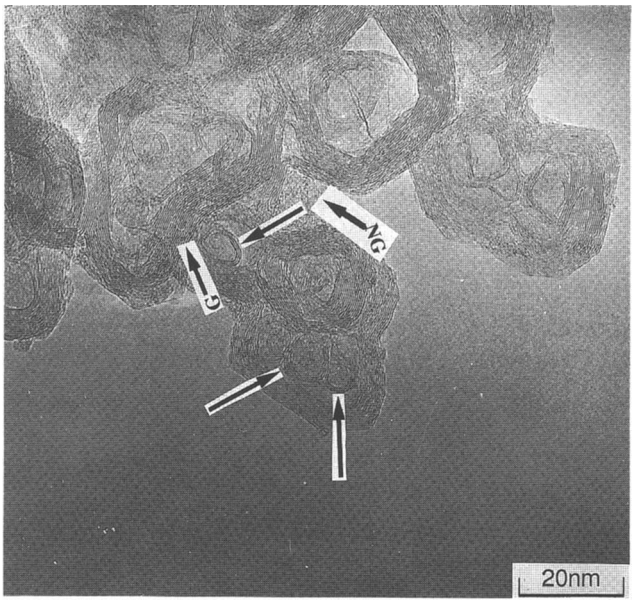

(b)

FIG. 4. High resolution TEM overview (a) and close-up (b) images of laser black particles heated to a HTT = 2850 °C in Ar. Indicated by arrows (b) are curved graphitic planes consisting of only a few layers of carbon atoms. Labels G and NG point to graphitized and nongraphitized regions, respectively.

B. BET and elemental analysis

Common to many types of carbon blacks,[2,22] significant particle agglomeration and possible sintering between the particles were also observed in our laser black particles. Using the standard N_2 BET technique, we determined a value ~50 m^2/g for the specific surface area for the as-synthesized carbon blacks. This value is slightly lower than 70 m^2/g reported for a typical acetylene black[22] and several other industrial carbon blacks.[2,21] It is also a factor of two lower than the theoretical total surface area for a powder comprised of 30 nm spherical particles (~100 m^2/g). The reduced surface area is consistent with the observation of particle agglomeration. Standard elemental analysis was applied to our laser black samples to determine the relative composition of Fe, C, and H. The results of a typical analysis yield a relative composition $C_{10}Fe_{0.01}H_{1.2}$ for the particles produced with a 6 mm nozzle and $C_{10}Fe_{0.03}H_{1.0}$ for the 9 mm nozzle. Therefore, the nozzle diameter essentially does not affect the composition of the laser black. It should be noted that the C:H ratio for both samples is about 8–10, similar to that of carbon particles formed in flames: C_8H, close to the ideal value C:H ~10 predicted for acetylene black using a polycondensation mode.[22] This value is significantly lower than that obtained experimentally for a typical acetylene black, which has C:H ~40.[22] Thus, laser pyrolysis produces a carbon black with a significant amount of hydrogen. No direct evidence for the existence of small iron particles in the laser black was found by TEM.

C. X-ray diffraction

Shown in Fig. 5 are the XRD results obtained with a Rigaku x-ray powder diffractometer using Cu K_α radiation (λ = 1.5418 Å) for the three laser black samples discussed above: (i) as-synthesized, (ii) HTT = 2000 °C, and (iii) HTT = 2850 °C. The diffraction pattern for

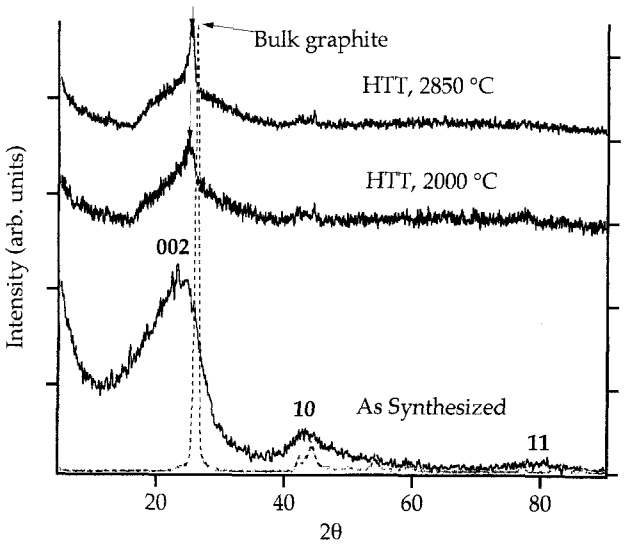

FIG. 5. XRD (Cu K_α, λ = 1.5418 Å) data for as-synthesized, HTT = 2000 °C, and HTT = 2850 °C laser black particles (solid lines). Data for bulk graphite (dashed line) are shown for comparison. The sharp peaks that appear in the HTT = 2000 and 2850 °C patterns indicate graphitization.

bulk graphite powders (Union Carbide) is also displayed in the figure for comparison. The diffraction pattern for the as-synthesized sample is similar to that of other types of carbon blacks.[22] Broad peaks 002, 100, and 110, indexed according to a convention of acetylene blacks, are observed for this sample. The two characteristic lengths L_a (along basal plane) and L_c (along c-axis) obtained for our laser black are 1.5 and 0.8 nm, respectively, as determined by the Debye–Scherrer equation from the full width at half maximum of the 100 and 002 peaks. The values of both L_a and L_c are less than that of most industrial carbon blacks, including those listed in Ref. 2, where $1.6 < L_a < 2.8$ nm, and $1.1 < L_c < 1.3$ nm. This result is consistent with our high resolution TEM images, which suggest that our nanoscale particles are more amorphous than those typically observed for industrial carbon blacks. As mentioned previously, such a high degree of disorder in our particles may well be associated with the exceedingly rapid growth and annealing (~1 ms) as the particles nucleate, grow, and pass out of the laser beam. For the as-synthesized particles, d_{002} is determined to be 0.37 nm from the 002 peak position using the Debye–Scherrer formula. This value is somewhat less than that measured directly from TEM image. This difference has been noted before, and attributed by Marsh *et al.*[23] to the different sensitivity of the two techniques to curved and flat carbon layers. It is known that bent graphitic planes generally have larger d_{002} spacing than those with flat parallel planes. TEM imagining reveals the spacing of both bent and flat graphitic layers, whereas XRD can obtain only the lattice spacing from regions of the sample with flat graphitic planes. Therefore, the average lattice spacing obtained by XRD analysis is consistently less than that measured directly by TEM.

In contrast to the TEM images (Figs. 2–4), which present only a very small portion of the sample, XRD data in Fig. 5 give an average picture of the entire particle batch. For the particles with HTT = 2000 °C, the powder pattern appears to contain two components. The first component, which has a sharp peak centered at $2\theta = 25.1°$ (down arrow), is a clear signature of graphitization. This 2θ value gives rise to $d_{002} = 0.355$ nm, less than that found for the as-synthesized sample. The second component is attributed to amorphous carbon black particles that have not responded to graphitization at 2000 °C. For the HTT = 2850 °C sample, this peak narrows further, and shifts slightly to a higher angle, and we find $d_{002} = 0.35$ nm. This d spacing is close to the value for turbostratic carbons (0.344 nm), yet still larger than the ideal value for graphite (0.335 nm), indicating that the graphitization in our particles is not complete, even at 2850 °C. The second component in the XRD spectrum is a broad shoulder centered around 25°, which appears to persist in the XRD data (Fig. 5) even for the particles with HTT = 2850 °C. The copresence of graphitized and nongraphitized components in the particles with HTT = 2850 °C is consistent with our TEM results. In Fig. 4(b), we indicate those graphitized and nongraphitized regions by labels G and NG, respectively. It is not clear what mechanism is responsible for such an inhomogeneous graphitization in our particles.

Figure 5 shows features for the HTT = 2850 °C particles: a sharp peak and a broad band (top curve). It is likely that the diffraction lines are broadened by the particles with inhomogeneous d_{002} lattice spacing. This makes it difficult to extract an accurate value for crystalline size L_c from the diffraction linewidth of both sharp and broad components. However, an order of magnitude estimate can be made for the value of L_c. Using the Debye–Scherrer formula, we estimate from the linewidth of the sharp component the L_c to be on the order of 5 nm. This value is close to the average shell thickness 7 nm, as measured from TEM pictures (Figs. 2–4). On the other hand, the linewidth of the broad component yields a L_c on the order of 1 nm, close to the value for our as-synthesized particles, which is 0.8 nm (see previous text). Though this value is approximate, it does provide a rough estimate for the crystalline size of nongraphitized regions. In this cases, it is difficult to obtain L_c for these disordered regions from TEM lattice images.

D. Raman scattering

In Fig. 6, we display Raman spectra at $T = 300$ K for the as-synthesized, 2000 °C and 2850 °C heat-treated

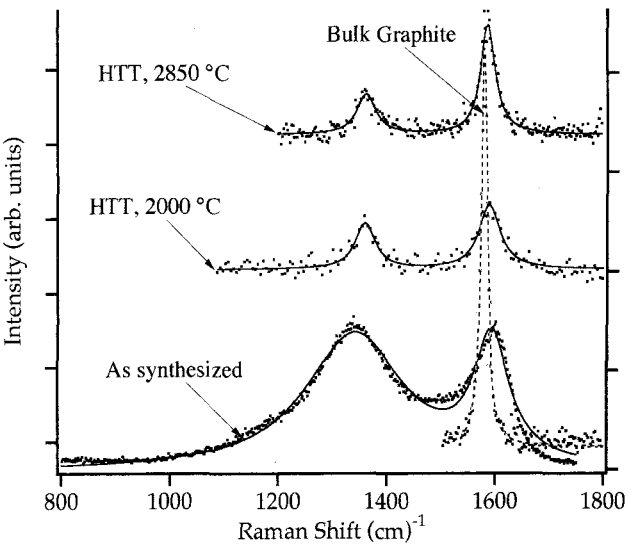

FIG. 6. Raman scattering ($T = 300$ K, Ar, $\lambda = 4880$ Å) results for as-synthesized, HTT = 2000 °C, and HTT = 2850 °C heat-treated laser black particles (dots). Bulk graphite results (dashed line) are shown for comparison. Solid lines represent a Lorentzian line shape fit to the data.

particles. The samples for the Raman scattering measurement are prepared by pressing the laser black into pellets. The experiments were carried out in a backscattering configuration where the argon laser beam (488 nm) was incident at 45° with respect to the pellet surface and polarized in the plane of incidence. Dry N_2 gas was blown gently over the sample surface during the measurement. A double-grating monochromator (SPEX 1500) and dry-ice-cooled photomultiplier (ITTFW130) were used to collect the spectra. The as-synthesized laser black particles exhibit a spectrum quite similar to that reported for glassy carbons, carbon blacks, charcoal, and carbon aerogels.[33,35,36,41,42] The broad peak at $\sim$1590 cm^{-1} is identified with the well-known E_{2g_2} mode of graphite, upshifted by $\sim$10 cm^{-1} from the position 1582 cm^{-1} reported for single-crystal graphite.[34] The broadband at 1340 cm^{-1} is identified with symmetry-forbidden modes associated with the maximum in the graphite density of states, activated by lattice disorder and/or small crystallite size. The Raman bands were fitted to a Lorentzian line shape to extract peak positions (ω_m), linewidths (Δ_m), and relative peak intensities (I_m). The ratios of the integrated intensities I_{1580}/I_{1340} for the as-synthesized and heat-treated samples were also calculated and used to estimate L_a. The results of the line shape analysis are summarized in Table I.

For the as-synthesized laser black (Table I), we find that the disorder-induced line (at 1340 cm^{-1}) is downshifted by 20 cm^{-1} and the E_{2g_2} mode (1594 cm^{-1}) is upshifted by 12 cm^{-1}, respectively, from their positions in polycrystalline graphite. The peak positions and full widths at half maximum intensity for these two bands are very close to that reported for glassy carbons prepared by chemical reaction of organic compounds.[43] The crystalline size L_a = 1.4 nm as determined from Raman spectra agrees well with the value (L_a = 1.5 nm) obtained by analyzing the x-ray diffraction line (100) using the Debye–Scherrer formula, as described previously. However, this agreement is fortuitous, since in this range, it is difficult to extract accurate L_a values from the Raman data.[36] It is clear from Table I that, upon annealing the laser black at elevated temperatures, the width of the E_{2g_2} mode decreases, indicating graphitization. This reduction in linewidth is accompanied by a reduction in the relative intensity ratio I_{1340}/I_{1590}, as expected. Furthermore, the peak positions appear to approach the values of polycrystalline graphite (Fig. 6 and Table I). The Raman data are therefore consistent with our XRD results, as described previously. From the I_{1580}/I_{1340} ratio we found that the in-plane crystalline size L_a increases from 1.4 nm in the as-synthesized laser black to 9 nm when annealed at HTT = 2850 °C. For the samples with HTT = 2000 °C and HTT = 2850 °C, L_a is measured in this study only by Raman scattering. For these two samples, the XRD peaks (10) are too weak to be used for the determination of the linewidth.

IV. KOH ACTIVATION

About 1.8 g of sample produced with a 9 mm nozzle was mixed with 8.6 g of KOH and 50.4 g of H_2O and a few drops of methanol at room temperature. The mixture was then heated to 850 °C at a rate of 15 °C/min in an atmosphere of flowing nitrogen, and the system was maintained at this temperature for 1 h before cooling. The solid product was leached with distilled water to a final pH = 6 and vacuum dried at 110 °C before analysis for pore size distribution. Information on the carbon pore structure was derived from nitrogen adsorption isotherms[45] obtained at 77 K on a Coulter Omnisorb 100CX apparatus; the micropore volume W_0 and the average width of the slit-shaped pores was determined using the Dubinin–Raduskevich equation.[44] Specific surface areas were obtained from the adsorption isotherms using the (Brunauer–Emmett–Teller)[45] BET equation. Mesopore surface areas were obtained using the α_s method[45]; standard isotherm data were taken from Rodriguez-Reinoso *et al.*[46] Using this method of analysis, the as-synthesized carbon particles were found to have BET surface areas in the range of 50 m^2/g, typical of carbon blacks.

The KOH activation process described above increased the BET surface area to 674 m^2g^{-1}. Such an enhancement of surface area is attributed to the formation of an internal micropore structure. High resolution TEM lattice images for as-synthesized and KOH activated carbon particles are shown in Figs. 7(a) and 7(b), respectively. What may be pore structures at the surface of the activated particles stemming from KOH activation are marked in Fig. 7(b) by A, B, C, and D. Similar pore structures in TEM images have been

TABLE I. Parameter values extracted from Raman scattering spectra.

	Disorder-induced			Raman-allowed			
	ω_m (cm^{-1})	I_m	Δ (cm^{-1})	ω_m (cm^{-1})	I_m	Δ (cm^{-1})	In-plane crystalline size L_a (nm)
As-synthesized	1341	184	219	1594	163	77	1.4
2000 °C	1360	61	44	1589	85	46	6.5
2850 °C	1362	53	42	1586	146	32	9.2

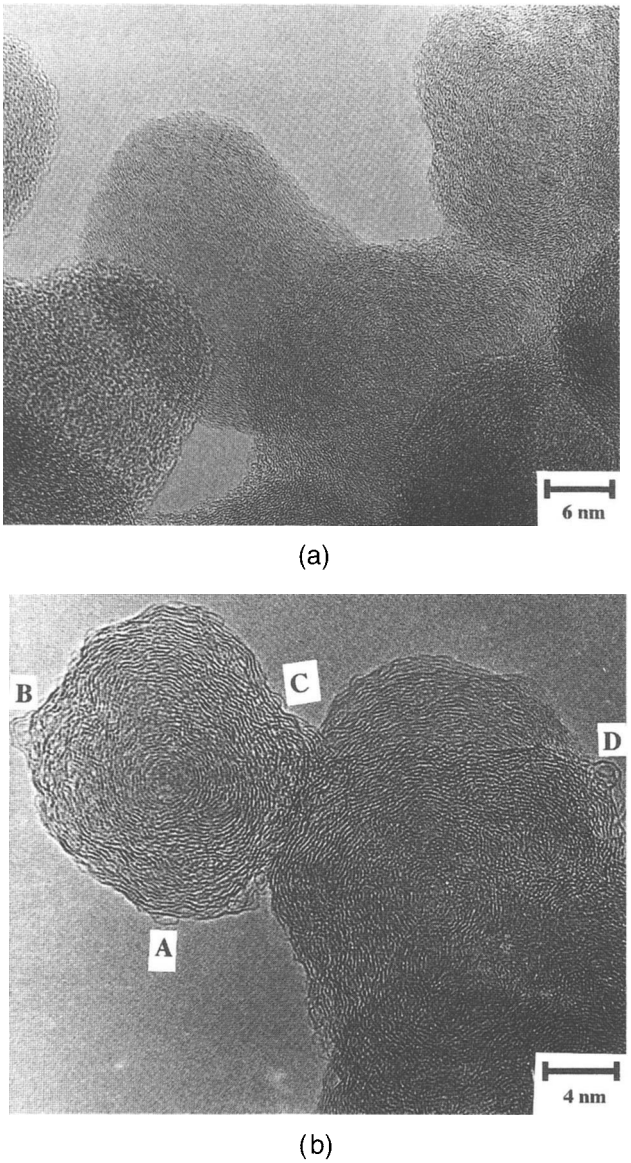

FIG. 7. High resolution TEM images of (a) as-synthesized (S_g = 50 m^2/g) and (b) KOH activated (S_g ~ 700 m^2/g) laser black particles. A few micropore structures, as marked in Fig. 7(b) by A, B, C, and D, are observed clearly under high resolution.

observed in the activated carbons with a specific surface area of 2000 m^2/g.[47] In our laser particles, these pores may be responsible for a factor of 10 increase in the surface area. It appears that the KOH-activated particles [Fig. 7(b)] exhibit regions with a more extensive plane alignment than observed for the as-synthesized laser blacks [Fig. 7(a)]. At the same time, the spacing between parallel layers appears to be greater after KOH activation. It is suggested that the mechanisms that give rise to the development of internal porosity also lead to an increase in plane alignment. However, this cannot be considered to be graphitization in the strict sense of the word, because of the low reaction temperature (850 °C) and the wide spacing of the carbon layers (large d_{002}) in the KOH-activated laser black.

Pores in activated carbons are divided by convention into three categories according to their diameter[44]: micropores $d < 2$ nm, mesopores 2 nm $< d <$ 50 nm, and macropores $d > 50$ nm. The adsorptive capacity in activated carbons stems primarily from micropores, and to some extent from mesopores, while there is negligible adsorption in macropores. The pore size distribution of the activated nanoparticles differs from what is normally achieved by KOH activation of materials such as mesocarbon, microbeads[48] from coal tar pitch, and bituminous coals. In these carbons, highly microporous materials are developed with low mesopore surface areas (in the range of 10–50 m^2/g).[48,49] In the case of the nanoparticles, the mesopore surface area is as high as 187 m^2/g^{-1}. The average width of the slit-shaped micropores, L, was 1.1 nm, which is within the range of that normally found in studies of KOH activation of coal and pitches.[48,50]

V. CONCLUSIONS

We have produced a carbon black with a mean particle diameter of 30 nm using CO_2 laser pyrolysis of mixtures of $C_2H_4 : C_6H_6 : Fe(CO)_5$. Variation of the composition of the mixture suggests that the C_2H_4 serves primarily as a chemically passive gas which absorbs the energy from the laser beam to drive the reaction. The Fe-carbonyl decomposes to form small Fe or Fe-carbide particles which catalyze the production of laser black from the benzene feed. Chemical analysis indicates a relatively high ratio of H/C ~0.1. The as-synthesized particles are nearly spherical, amorphous, and exhibit in TEM images only a slight tendency to graphitize. Heat treatment of the as-synthesized particles to 2850 °C transforms most of the particles to a faceted, polyhedral shape with hollow polyhedral cores. Each facet is a nanoplate of turbostratic graphite as inferred from TEM, XRD, and Raman scattering. Finally, chemical treatment of the laser black in KOH at 850 °C enhances the BET surface area by a factor of ~10 to 700 m^2/g. Approximately 580 m^2/g of this surface area was attributed to the presence of micropores ($d < 2$ nm), whereas the remainder of the area was identified with an unusually large contribution from mesopores (2 nm $< d <$ 50 nm).

ACKNOWLEDGMENTS

The U.K. authors thank the U.S. Department of Energy (DE-FC22-93PC93053) for support. The work at MIT was supported by the NSF (DMR-95-10093).

REFERENCES

1. J. Lahaye and G. Prado, in *Chemistry and Physics of Carbon*, edited by P. L. Walker (Marcel Dekker, Inc., New York, 1978), Vol. 14, p. 167.

2. *Carbon Black,* edited by J-B. Donnet, R.C. Bansal, and M-J. Wang (Marcel Dekker, Inc., New York, 1993).
3. J.A. Howe, J. Chem. Phys. **39**, 1362 (1963).
4. Y.P. Yampolskii, Y.V. Maximov, N.P. Novikov, and K.P. Lavrovskii, Khim, Vys. Energ. **4**, 283 (1970).
5. J.T.D. Maleissye, F. Lempereur, and C. Marsal, C.R. Acad. Sci., Paris, Ser. **275**, 1153 (1972).
6. M.S. Dresselhaus, G. Dresselhaus, and P.C. Eklund, J. Mater. Res. **8**, 2054–2097 (1993).
7. J.S. Haggerty, in *Laser-induced Chemical Processes,* edited by J.I. Steinfeld (Plenum Press, New York, 1981).
8. P.C. Eklund, X-X Bi, and F.J. Derbyshire, Preprints of Fuel Division, American Chemical Society **37** (4), 1781 (1992).
9. X-X. Bi, B. Ganguly, G.P. Huffman, F.E. Huggins, M. Endo, and P.C. Eklund, J. Mater. Res. **8**, 1666 (1993).
10. P.C. Eklund, R. Ochoa, X-X. Bi, M.S. Dresselhaus, and S. Bandow, Energeia **5** (6), 1 (1994).
11. X-X. Bi, K. Chowdhury, W. Lee, S. Bandow, M.S. Dresselhaus, and P.C. Eklund, Proc. Mater. Res. Soc. (1995, in press).
12. J.M. Stencel, P.C. Eklund, X-X. Bi, and F.J. Derbyshire, Catalysis Today **15**, 285 (1992).
13. P.A. Tesner, M.M. Polyakova, and S.S. Mikheeva, Tr. Vses. Nauk. Issled. Inst. Priz. Gazov **40/48**, 8 (1969).
14. S.S. Abadzev, P.A. Tesner, and U.V. Smevchan, Gazov. Prom. **14** (10), 36 (1969).
15. B.N. Al'Thuler and P.A. Tesner, Gazov. Prom. **6**, 41 (1969).
16. D.V. Fedoseev and S.P. Vnukov, Dok. Akad. Nauk. SSSR [Sov. Phys. Dokl.] **209** (5), 1162 (1973).
17. B.E. Warren, J. Chem. Phys. **2**, 551 (1934).
18. B.E. Warren, Phys. Rev. **59**, 693 (1941).
19. R.E. Franklin, Acta Crystallogr. **3**, 107 (1950).
20. R.E. Franklin, Acta Crystallogr. **4**, 253 (1951).
21. X. Bourrat, Carbon **31** (2), 287–302 (1993).
22. Y. Schwob, in *Chemistry and Physics of Carbon,* edited by P.L. Walker and P.A. Thrower (Marcel Dekker, Inc., New York and Basel, 1979), Vol. 15, p. 109.
23. P.A. Marsh, A. Voet, T.J. Mullens, and L.D. Price, Carbon **9**, 797–805 (1971).
24. R.D. Heidenreich, W.M. Hess, and L.L. Ban, J. Appl. Crystallogr. **1**, 1 (1968).
25. L.L. Ban and W.M. Hess, Extended Abstracts *10th Biennial Conference on Carbon* (Defense Ceramic Information Center, Columbus, OH, 1971), p. 159.
26. L.L. Ban, Chemical Society of London **1**, 54 (1972).
27. C.E. Hall, J. Appl. Phys. **19**, 271 (1948).
28. H.P. Boehm, Z. Anorg. U. Allgem. Chem. **297**, 315 (1958).
29. V.I. Kasatotchkine, V.M. Loukianovitch, N.H. Popov, and K.V. Tchmoutov, J. Chem. Phys. **37**, 822 (1960).
30. R.D. Heidenreich, Bell System, Tech. J. **47**, 265 (1968).
31. J.B. Donnet and J.C. Bouland, Rev. Gen. Caout. **41**, 407 (1964).
32. F.A. Heckman, Rubber Chem. Technol. **37**, 1245 (1964).
33. F. Tuinstra and J.L. Koenig, J. Chem. Phys. **53** (3), 1126–1130 (1970).
34. M.S. Dresselhaus and G. Dresselhaus, in *Light Scattering in Solids III, Topics in Applied Physics* (Springer-Verlag, Berlin, 1982), Vol. 51, p. 3.
35. D.S. Knight and W.B. White, J. Mater. Res. **4**, 385 (1989).
36. A.W.P. Fung, Z.H. Wang, K. Lu, M.S. Dresselhaus, and R.W. Pekala, J. Mater. Res. **8**, 1875 (1993).
37. R.B. Anderson, H. Koebel, and M. Ralek, *The Fischer-Tropsch Synthesis* (Academic Press, London, 1984), pp. 140–145.
38. R.T.K. Baker, P.S. Harris, R.B. Thomas, and R.J. Waite, J. Catalysis **30**, 86–96 (1973).
39. R.C. Bansal and J.B. Donnet, *Carbon Black Science and Technology,* edited by J.B. Donnet, R.C. Bansal, and M.J. Wang (Marcel Dekker Inc., New York, 1993), pp. 67–88.
40. H. Palmer and C. Cullis, in *Chemistry and Physics of Carbon,* edited by P.L. Walker (Marcel Dekker, New York, 1965), Vol. 1, p. 265.
41. M. Nakamizo, R. Kammereck, and P.L. Walker, Carbon **12**, 259–267 (1974).
42. Y. Sato, M. Kamo, and N. Setaka, Carbon **16**, 279–280 (1978).
43. M. Nakamizo, Carbon **29**, 757–761 (1991).
44. R.C. Bansal, J.B. Donnet, and F. Stoeckli, *Active Carbon* (Marcel Dekker Inc., New York, 1988), p. 139.
45. S.J. Gregg and K.S.W. Sing, *Adsorption, Surface Area and Porosity,* 2nd ed. (Academic, London, 1982), pp. 94–100.
46. F. Rodriguez-Reinoso, J.M. Martin-Martinez, C.P. Prado-Burguette, and B. McEnaney, J. Phys. Chem. **91**, 515–516 (1987).
47. M. Endo, K. Oshida, K. Takeuchi, Y. Sasuda, K. Matsubayashi, and M.S. Dresselhaus, Trans. IEICE Japan **J77-II**, 139 (1994).
48. M. Jagtoyen, C. Toles, and F. Derbyshire, Preprints of ACS, Denver, Colorado, March 28–April 2, 1993.
49. T. Kasuh, D.A. Scott, and M. Morl, Proceedings Carbon '88, Newcastle, England (IOP Publishing Ltd., 1988).
50. T. Otowa, in *Proc. Adsorptive Separation,* May 20–21, 1991, Tokyo, Japan, edited by M. Suzuki (1991).